Journal of The Electrochemical Society, **151** (3) A456-A462 (2004)
0013-4651/2004/151(3)/A456/7/$7.00 © The Electrochemical Society, Inc.

Solvent Diffusion Model for Aging of Lithium-Ion Battery Cells

Harry J. Ploehn,[z] Premanand Ramadass,[*] and Ralph E. White[**]

Department of Chemical Engineering, University of South Carolina, Swearingen Engineering Center, Columbia, South Carolina 29208, USA

This work presents a rigorous continuum mechanics model of solvent diffusion describing the growth of solid-electrolyte interfaces (SEIs) in Li-ion cells incorporating carbon anodes. The model assumes that a reactive solvent component diffuses through the SEI and undergoes two-electron reduction at the carbon-SEI interface. Solvent reduction produces an insoluble product, resulting in increasing SEI thickness. The model predicts that the SEI thickness increases linearly with the square root of time. Experimental data from the literature for capacity loss in two types of prototype Li-ion cells validates the solvent diffusion model. We use the model to estimate SEI thickness and extract solvent diffusivity values from the capacity loss data. Solvent diffusivity values have an Arrhenius temperature dependence consistent with solvent diffusion through a solid SEI. The magnitudes of the diffusivities and activation energies are comparable to literature values for hydrocarbon diffusion in carbon molecular sieves and zeolites. These findings, viewed in the context of recent SEI morphology studies, suggest that the SEI may be viewed as a single layer with both micro- and macroporosity that controls the ingress of electrolyte, anode passivation by the SEI, and cell performance during initial cycling as well as long-term operation.
 [DOI: 10.1149/1.1644601]

Manuscript submitted April 15, 2003; revised manuscript received September 27, 2003. Available electronically February 11, 2004.

Various mechanisms for capacity loss in Li-ion cells, including electrode passivation, electrolyte decomposition, active material dissolution, phase change, overcharge, self-discharge, and several other phenomena have been reviewed in the literature.[1-6] The irreversible capacity loss that occurs during the first few cycles of charge-discharge is primarily due to the formation of a passive film over the negative electrode,[7-14] known as the solid-electrolyte interface (SEI). Formation of the SEI consumes lithium that would otherwise participate in charge-discharge cycling. This is a necessary cost, for the SEI serves as a crucial passivating layer that isolates the negative electrode from the electrolyte, minimizing further reduction of electrolyte components. At the same time, the SEI should permit facile Li^+ transport between the negative electrode and the electrolyte. Thus the structure and transport properties of the SEI are critical because they govern electrode surface properties as well as long-term performance metrics such as shelf life, cycle life, and capacity fading.

The relationship among electrolyte composition, SEI structure, and cell performance has been reviewed extensively by Aurbach and co-workers.[10-14] In general, reduction of ''good'' electrolytes produces species that adhere strongly to the graphite, producing thin, dense SEI films that have low solvent permeability. Furthermore, good SEI films should have mechanical pliability to withstand volume changes associated with Li^+ intercalation-deintercalation, or at least the ability to rapidly heal, via further solvent reduction, should any breaches occur. Reduction of ''poor'' electrolytes leads to porous SEI films (due to poor mechanical integrity and formation of particulate or dendritic morphologies) that may permit continuing reduction or solvent cointercalation.

Recent visualization studies of SEI morphology by scanning electron microscopy (SEM),[15] transmission electron microscopy (TEM),[16] scanning tunneling microscopy (STM),[17,18] and atomic force microscopy (AFM)[19] support this physical picture. SEM, TEM, and AFM images of graphitic carbon anodes cycled in ''good'' electrolytes (*e.g.*, 1.0 M $LiPF_6$ or $LiClO_4$ in 1:1 by weight mixtures of ethylene carbonate and dimethyl carbonate, EC and DMC) provide direct visual evidence of SEIs having lateral uniformity across the carbon surface with thicknesses up to tens of nanometers and little gross porosity. Images of SEIs cycled or stored in other electrolytes (especially mixtures of propylene carbonate, PC, with EC) show clear evidence of porosity. These studies help us understand the mechanisms of SEI formation and first cycle capacity loss, especially why certain electrolyte compositions are ''good'' or ''poor,'' in terms of SEI morphology.

This understanding may also help explain long-term capacity fading which occurs even in Li-ion batteries employing optimal electrolytes. SEM images[15] indicate that the SEI morphology evolves during long-term storage of charged anodes. Electrochemical impedance spectroscopy data for the same samples imply that SEI roughness or porosity increases over time, while discharge measurements document capacity loss after storage. We believe that SEI porosity plays an important role in Li-ion capacity fade, for both charge-discharge cycling and self-discharge under storage conditions. This concept is consistent with Aurbach's picture[13,14] of capacity fading associated with graphite electrodes in ''good'' electrolytes, which includes initial formation of a uniform SEI, damage with increased SEI porosity due to lithium transport through the SEI, and finally, SEI repair through additional solvent reduction. We believe that all SEIs, including those formed in ''good'' electrolytes, have a significant level of porosity (or permeability) that permits the ingress of electrolyte components (solvents and/or solvated ions). This hypothesis, if correct, would provide a common physical basis (in terms of SEI composition and morphology) for understanding both the initial quality of the ''as-formed'' SEI and its long-term role in capacity fading and cell cycle life.

The key issue, the mechanism of SEI growth and repair, was addressed by Broussely *et al.*[20,21] in a recent study of capacity fading of Li-ion cells employing graphite anodes and organic electrolytes. Cells of various designs were initially subjected to a few charge-discharge cycles to passivate the carbon anodes. The cells were then stored for up to a year in the fully charged state at a voltage held constant by maintaining a small trickle current (''float potential''). They measured the capacity loss as a function of storage time, temperature, and float potential. They inferred from their data that electrolyte reduction on the carbon anode is the most important contributor to capacity loss under float potential storage conditions. They observed that the capacity loss increases with the square root of time, which they attribute to the production and deposition of an SEI that limits the electrolyte reduction rate.

In order to rationalize these observations, Broussely *et al.*[20] adapted Peled's model[7-9] of SEI growth on lithiated carbon anodes limited by SEI electronic conductivity. This model postulates[20] that the rate of lithium loss (in terms of moles of lithium lost, $\mathcal{N}_L$) is proportional to SEI electronic conductance (X)

$$\frac{d\mathcal{N}_L}{dt} = kX = \frac{k\chi A_{anode}}{L} = \frac{B}{L} \qquad [1]$$

* Electrochemical Society Student Member.
** Electrochemical Society Fellow.
[z] E-mail: Ploehn@engr.sc.edu

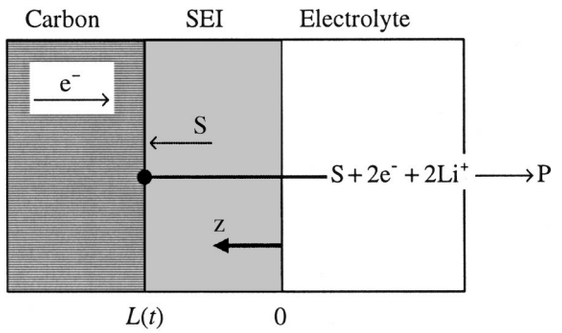

Figure 1. Schematic diagram of SEI growth via solvent diffusion through the SEI.

where k is a proportionality constant, χ is the SEI specific conductivity (dependent only on temperature), A_{anode} is the anode surface area, and $B = k\chi A_{\text{anode}}$ is constant. The SEI thickness, $L(t)$, can be expressed as

$$L = L_0 + A\mathcal{N}_L \quad [2]$$

where L_0 is the initial SEI thickness after the first few charge-discharge cycles, and A is another empirical parameter independent of both time and temperature. This expression assumes that lithium, electrons, and electrolyte react to produce an insoluble product P with constant composition and average molar volume.

Combining Eq. 1 and 2, integrating subject to the initial condition of $\mathcal{N}_L = 0$ at time $t = 0$, and rearrangement yield

$$t = \frac{A}{2B}\mathcal{N}_L^2 + \frac{L_0}{B}\mathcal{N}_L \quad [3]$$

Broussely *et al.*[20] also assumed, implicitly, that the cell capacity is proportional to the available number of moles of lithium, $\mathcal{N}_0 - \mathcal{N}_L$, with $\mathcal{N}_0$ denoting the initial number of moles of lithium available for cycling. Then the fractional capacity loss can be expressed as $x(t) \equiv \mathcal{N}_L/\mathcal{N}_0$ and Eq. 3 becomes

$$t = \frac{A'}{2B'}x^2 + \frac{L_0}{B'}x \quad [4]$$

in accord with Eq. 5 of Ref. 20, except with $A' \equiv A\mathcal{N}_0$ and $B' \equiv B/\mathcal{N}_0$.

This quadratic relationship between time and SEI thickness (or its surrogate, fractional capacity loss) is by no means unique. In this work, we interpret the data of Broussely *et al.*[20] in terms of a one-dimensional model of solvent diffusion through a porous SEI. Upon reaching the carbon/SEI interface, solvent (EC) undergoes two-electron reduction, thus growing the SEI at the internal interface. This scenario is consistent with the view that a robust SEI should be able to heal itself as damage occurs during charge-discharge cycling. As the SEI thickness increases, the solvent diffusion rate decreases, thus slowing the rate of SEI growth and fractional capacity loss. In fact, the solvent diffusion-limited model presented later leads to fractional capacity loss increasing with the square root of time, in accord with the data of Broussely *et al.*[20]

Model Development

Assumptions.—Figure 1 presents a schematic diagram of the Li-ion half-cell illustrating the transport processes and reactions occurring near the surface of a carbon anode under float charge conditions. This diagram reflects several assumptions. First, we assume planar symmetry of the anode and consider only transport in one spatial Cartesian coordinate, valid away from the edges of the anode. Frame indifference[22] enables us to work in reference frame in which the SEI-electrolyte interface is stationary, located for convenience at $z = 0$.

The electrolyte consists of one or more solvent components and a lithium salt. The reduction of various alkyl carbonates with lithium and lithiated carbon has been studied extensively. Experiments[13,14,23,24] generally agree that among the various alkyl carbonates used in prototype Li-ion batteries, EC is the most reactive. Moreover, theory[25] provides additional support for a reaction mechanism involving two-electron reduction of EC to produce either Li_2CO_3 or lithium alkyl carbonates at low or high EC concentrations, respectively. For our model, we assume that the reaction of one solvent component (S) dominates. This component undergoes two-electron reduction at the carbon-SEI interface via

$$\mathrm{S} + 2\mathrm{e}^- + 2\mathrm{Li}^+ \rightarrow \mathrm{P} \quad [5]$$

producing an insoluble product (P) with constant molar density (c_P). With respect to the experiments of Broussely *et al.*,[20] we assume that S corresponds to EC, and P to Li_2CO_3. Within the SEI phase, component S is the only mobile component and has a constant effective diffusivity (D_S). Moreover, we shall assume that S is dilute within the SEI so that $c_S \ll c_P$. Electrons and lithium cations are available in excess at the carbon-SEI interface.

Transport equations.—Under the assumptions described in the previous section, the SEI growth problem is very similar to that of the growth of silica layers on silicon surfaces limited by the diffusion of molecular oxygen through the growing silica layer.[26] Assuming a constant c_P and a reference frame in which the SEI is stationary, the flux of P is zero and the differential mass balance for P is satisfied identically. The differential mass balance for the solvent in the SEI phase is

$$\frac{\partial c_S}{\partial t} + \frac{\partial N_{z,S}}{\partial z} = 0 \quad [6]$$

Assuming Fickian diffusion[22] of the solvent with D_S as the effective binary diffusivity of S in P, we have

$$N_{z,S} = x_S \sum_I N_{z,I} - cD_S\frac{\partial x_S}{\partial z} \quad [7]$$

where c denotes the total molar concentration and x_I the mole fraction of component I (S or P). Simplification of Eq. 7 is not trivial because $c(z,t)$ is not constant. Recognizing that $c = c_S + c_P$, $x_S \equiv c_S/c$, and that only the solvent has a nonzero flux, one may ultimately show that Eq. 7 reduces to

$$N_{z,S} = -D_S\frac{\partial c_S}{\partial z} \quad [8]$$

Substitution of Eq. 8 into Eq. 6 yields

$$\frac{\partial c_S}{\partial t} = D_S\frac{\partial^2 c_S}{\partial z^2} \quad [9]$$

which governs solvent diffusion through the SEI.

Boundary conditions for this moving boundary problem are easily derived from jump mass balances[22] for S and P at the carbon/SEI interface, yielding

$$\text{At } z = L(t): \quad -N_{z,S} = \frac{r_S^\sigma}{M_S} - c_S\frac{dL}{dt} \quad [10]$$

and

$$\text{At } z = L(t): \quad 0 = \frac{r_P^\sigma}{M_P} - c_P\frac{dL}{dt} \quad [11]$$

respectively. Based on the stoichiometry of Eq. 5, the molar production rates (r_1^σ/M_1) of the various species are related by

$$\frac{r_P^\sigma}{M_P} = -2\frac{r_{e^-}^\sigma}{M_{e^-}} = -2\frac{r_{Li^+}^\sigma}{M_{Li^+}} = -\frac{r_S^\sigma}{M_S} \quad [12]$$

Adding Eq. 10 and 11 and eliminating the reaction rates using Eq. 12 gives

$$\text{At } z = L(t): \quad \frac{dL}{dt} = \frac{N_{z,S}}{(c_P + C_S)} \approx \frac{N_{z,S}}{c_P} \quad [13]$$

The second equality follows from the key assumption $c_S \ll c_P$. Substituting this expression into Eq. 11 gives

$$\text{At } z = L(t): \quad N_{z,S} = \frac{r_P^\sigma}{M_P} = -\frac{r_S^\sigma}{M_S} \quad [14]$$

In turn, substituting this expression into Eq. 10 leads to the conclusion that

$$\text{At } z = L(t): \quad c_S \approx 0 \quad [15]$$

Thus all S that diffuses through the SEI is consumed at the carbon/SEI interface.

We assume local equilibrium at the SEI/electrolyte interface implies a relationship between the concentrations of S in the SEI and the electrolyte

$$\text{At } z = 0: \quad c_S = c_{eq} \quad [16]$$

Lacking detailed thermodynamic information about partitioning at this interface, we assume that c_{eq} equals the concentration of the reactive solvent component S in the electrolyte solution.

Analytical solution.—Equations 9, 15, and 16 are the final set of equations to be solved. The same set of equations has been solved previously[22,26] in the context of silicon oxidation. Dimensional analysis shows that these equations can be solved through the similarity transformation of the form

$$u \equiv \frac{z}{\sqrt{4D_S t}} \quad [17]$$

without the need for an initial condition. Employing this change of variable, Eq. 9 becomes

$$\frac{d^2c_S}{du^2} + 2u\frac{dc_S}{du} = 0 \quad [18]$$

with the boundary conditions

$$\text{At } u = \lambda: \quad c_S \approx 0 \quad [19]$$

and

$$\text{At } u = 0: \quad c_S = c_{eq} \quad [20]$$

In Eq. 19, we have

$$\lambda = \frac{L(t)}{\sqrt{4D_S t}} \quad [21]$$

Since $c_S(\lambda) = 0$ from Eq. 19, λ must be a constant.

The solution of Eq. 18 consistent with Eq. 19 and 20 is[22,26]

$$c_S(z,t) = c_{eq}\left(1 - \frac{\text{erf}(u)}{\text{erf}(\lambda)}\right) \quad [22]$$

where λ may be found from the solution of

$$\lambda = \frac{c_{eq}}{\sqrt{\pi}c_P}\frac{\exp(-\lambda^2)}{\text{erf}(\lambda)} \quad [23]$$

Equation 21 gives

$$L(t) \equiv 2\lambda\sqrt{D_S t} \quad [24]$$

As one might expect for diffusion-limited film growth, the SEI thickness increases with the square root of time.

In order to compare the predicted trend, Eq. 24, with experimental data for capacity loss, we must invoke some additional assumptions. First, cell capacity is proportional to the moles of Li available for cycling, and all capacity loss must be due to Li consumption associated with electrolyte reduction. This produces an insoluble product, *P*, having constant composition and molar volume. Under these conditions, a lithium mass balance gives

$$x(t) = \frac{\mathcal{N}_L(t)}{\mathcal{N}_0} = \frac{Z_P c_P A_{anode}}{\mathcal{N}_0} L(t) = \frac{2Z_P c_P A_{anode}\lambda}{\mathcal{N}_0}\sqrt{D_S t} \quad [25]$$

for the fractional capacity loss $x(t)$, where Z_P is the stoichiometric coefficient of Li in P. If we know (or assume) the electrolyte composition and the molar volume of P in the SEI, the values of c_{eq}, c_P, λ (from Eq. 23), and Z_P are all determined. The anode area (A_{anode}) is a cell design parameter, and the initial capacity ($\mathcal{N}_0$) is a measured value. If experimental data for $x(t)$ is linear when plotted *vs.* $\sqrt{t}$, then we may extract D_S from the slope of this plot.

Results and Discussion

Capacity loss.—Broussely *et al.*[20] measured the capacity loss of various prototype Li-ion cells as functions of time, storage temperature, and float potential. Table I summarizes the design details of these cells, including the measured values of initial capacity $\mathcal{N}_0$. Figure 2 shows data (symbols from Ref. 20, Fig. 5, cell 2) for capacity loss *vs.* $\sqrt{t}$ for HE prototype cells stored at 30 and 60°C and at a float potential of 3.8 V. The solid curves are one parameter linear fits of the data. Likewise, Fig. 3 shows data (symbols from Ref. 20, Fig. 1) for capacity loss *vs.* $\sqrt{t}$ for MP prototype cells stored at various temperatures and at a float potential of 3.9 V. Despite the scatter in the data, one-parameter linear regression again provides a satisfactory fit. Table II shows linear correlation coefficients (R^2) for the two-parameter linear regressions reported by Broussely *et al.*[20] (on data in their Fig. 6 and 7) as well as our corresponding one-parameter regressions (our Figures 2 and 3). The overall quality of the linear regressions of the capacity loss data in Fig. 2 and 3 demonstrates that the solvent diffusion model provides a satisfactory description of capacity loss in these Li-ion cells. Considering that the solvent diffusion model has only one adjustable parameter, the fidelity of this model is perhaps better than that of the two-parameter electronic conductivity model (Eq. 4) employed by Broussely *et al.*[20]

SEI thickness.—The solvent diffusion model can be used to estimate the SEI thickness and extract the solvent diffusivity from capacity loss data via Eq. 25. First, we assume that in the HE and MP prototype cells studied by Broussely *et al.*,[20] EC reduction produces Li_2CO_3 as the predominant product, so we use $Z_P = 2$ and $c_P = 2.11$ g/cm^3 in Eq. 25. Although Broussely *et al.*[20] identified the solvents used in the cells, they did not specify the mixing ratios, so we assumed the volume ratios shown in the lower part of Table I. The solvent compositions are used to calculate c_{eq} for EC in the mixture and thus λ from Eq. 23 (values given in Table I).

The final parameter required to estimate SEI thickness is the anode area, A_{anode}, representing the actual carbon surface area that is both electrochemically active and accessible to electrolyte. For composite carbon anodes typically based on graphite powders, values of A_{anode} are generally unknown. The area of the underlying

Table I. Published and assumed characteristics of the HE and MP prototype Li-ion cells studied by Broussely *et al.*[20]

Published characteristics[20]	HE prototype	MP prototype
Cell design	Cylindrical	Prismatic
Positive electrode	$LiNi_{0.91}Co_{0.09}O_2$	$LiCoO_2$
Negative electrode	Synthetic graphite	Synthetic graphite
Electrolyte salt	1.0 M $LiPF_6$	1.0 M $LiPF_6$
Electrolyte solvents	PC-EC-DMC	EC-DEC-DMC-VC
Rated capacity (Ah)	40	5
Storage temperatures	30 and 60°C	15, 30, 40, and 60°C
Float potentials	3.8 V	3.9 V
Capacity measurement	C/10 discharge at 60°C	C/5 discharge at 30°C
Initial capacity[a] (Ah)	50.93 (30°C, cell 2) 49.16 (60°C, cell 2)	4.98 (15°C) 4.98 (30°C) 4.96 (40°C) 5.01 (60°C)
Assumed characteristics		
Solvent volume ratio	1:1:1 PC-EC-DMC	1:1:1:0 EC-DEC-DMC-VC
c_{eq} (mol/cm^3)	2.636×10^{-3}	4.541×10^{-3}
λ	0.21168	0.27493
Anode current collector area[b] (m^2)	1.33	0.165
Carbon surface area,[b] A_{anode} (m^2)	173	21.5

[a] Initial capacity values from Ref. 20, Fig. 5 (HE prototypes) and Fig. 1 (MP prototypes).
[b] Estimated; see text.

current collector provides a lower bound on A_{anode} and would be appropriate if the carbon anode were a perfect sheet of highly ordered pyrolytic graphite (HOPG). At the other extreme, the carbon surface area obtained through gas absorption measurements [*e.g.*, Brunauer-Emmett-Teller (BET)] might serve as the upper bound on A_{anode}. However, it has been noted[27] that "the surface of a composite graphite electrode, which is accessible to the electrolyte, can be expected to differ considerably from the surface of a graphite powder... accessible to N_2 at 77 K." Here we use an order-of-magnitude estimate of A_{anode} to show that the resulting predictions of SEI thickness are in reasonable accord with other experimental observations.

First, we note that Broussely *et al.*[20] did not report, for any of their cells, the actual anode current collector areas, the two types of synthetic graphites they used, the loading of the active material, or any details about how the anodes were fabricated. Our previous studies[28,29] of commercial Li-ion cells indicate that anode area is, on average, directly proportional to rated capacity. From the rated capacities given in Table I, we used the same proportionality constant to estimate the values of the current collector areas given in the lower part of Table I. To estimate A_{anode} from the current collector areas, we need values of the carbon loading in the composite anode and the specific surface area of the active carbon. Lacking this information for the SAFT cells,[20] we instead used information from the work of Winter *et al.*[27,30] for estimation purposes. Based on carbon loadings[30] of 0.00923 g/cm^2 (*i.e.*, 1.2 mg/1.3 cm^2) and a specific surface area[27] of 1.41 m^2/g for the prismatic surface area of TIMREX KS75 graphite, we can easily convert the current collector areas into the estimates for A_{anode} given in the lower part of Table I.

The values (Table I) of Z_P, c_P, A_{anode}, (all assumed) and $\mathcal{N}_0$ (measured[20]) establish the proportionality between capacity loss, $x(t)$, and SEI thickness, $L(t)$, in Eq. 25. Figures 2 and 3 show, on secondary ordinate axes (right), estimates of $L(t)$ *vs.* $\sqrt{t}$ for the HE and MP prototype cells studied by Broussely *et al.*[20] The solvent diffusion model predicts, in all cases, SEI films growing to several tens of nanometers in thickness over time periods in excess of 1 year under float potential conditions. The lithium mass balance implicit

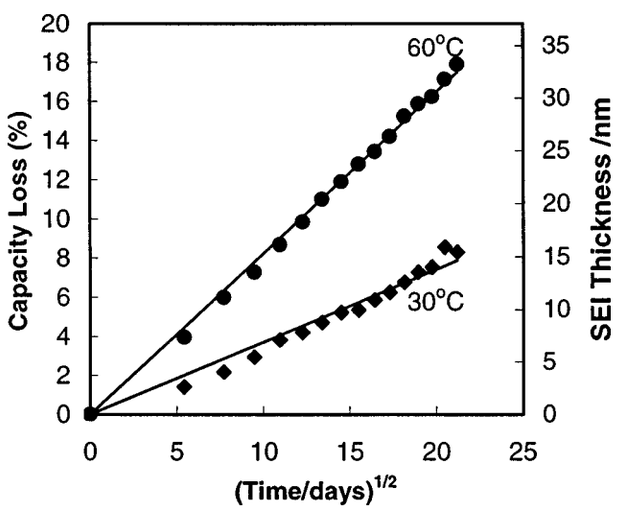

Figure 2. Measured capacity loss[20] and estimated SEI thickness as functions of time and temperature for HE prototype cells stored a float potential of 3.9 V.

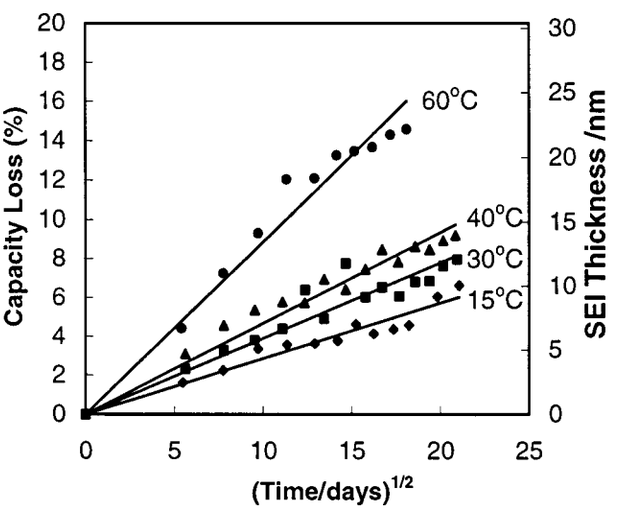

Figure 3. Measured capacity loss[20] and estimated SEI thickness as functions of time and temperature for MP prototype cells stored a float potential of 3.8 V.

Table II. Linear correlation coefficients for two-parameter linear regressions reported by Broussely *et al.*[20] (data in their Fig. 6 and 7) and for one-parameter regressions in this work (Fig. 2 and 3).

Cell prototype	Storage temp. (°C)	Linear correlation coefficient (R^2) Broussely *et al.*[20]	This work
HE	30	0.9965	0.9828
	60	0.9995	0.9980
MP	15	0.8605	0.8790
	30	0.9285	0.9377
	40	0.9238	0.9429
	60	0.9	0.9365

in Eq. 25, the assumption of insoluble reduction products, and the magnitude of the measured capacity losses dictate SEI film thicknesses of this magnitude. Unfortunately, we are not aware of any experimental data for SEI films formed under similar conditions that may be compared directly with the model predictions.

Recent AFM measurements of SEI films formed on HOPG after one or two charge-discharge cycles provide at least a qualitative basis for comparison. Hirasawa *et al.*[31] used AFM to estimate a minimum film thickness of 50-70 nm for the SEI formed on HOPG in 1.0 M Li_2ClO_4 + 1:1 EC-EMC solution during one charge-discharge cycle. Thicker particulate films, on the order of hundreds of nanometers, were implied by the measurements of Chu *et al.*[32] for HOPG in similar electrolytes. Interpretation of these early AFM measurements may be problematic because the SEI films may have been damaged due to excessive contact force. More recent, lower force AFM measurements by Alliata *et al.*[19] indicated film thicknesses in excess of 25 nm for SEIs formed over two charge-discharge cycles on HOPG in 1.0 M Li_2ClO_4 + 1:1 EC-DMC. These studies all suggest that relatively thick SEI layers form after just a few charge-discharge cycles.

The additional growth in thickness expected over months or years of self-discharge under float potential conditions has not been measured. However, if the initial formation of a 10-100 nm thick SEI is accompanied by a 10-20% initial capacity loss, then a subsequent 10% capacity loss during long-term self-discharge ought to produce SEI thickness growth of the same order of magnitude. Thus the SEI thicknesses predicted by the solvent diffusion model are reasonable, notwithstanding all of the assumptions required to generate the estimates. For a given value of capacity loss, the predicted SEI thickness would be smaller if some of the reduction products were soluble in the electrolyte. The predicted SEI thickness could be greater if the reduction product has a lower average molar density or significant porosity. The thickness varies most significantly with the true active carbon area, which depends on a host of material properties and the details of how the anode is fabricated.

Solvent diffusivity.—We may extract values of solvent diffusivity in the SEI from the slopes of the lines in Fig. 2 and 3 and the values of λ in Table I. The diffusivity values are given in Table III and depicted in an Arrhenius plot in Fig. 4. The diffusivity values in Table III, on the order of 10^{-23} m^2/s, are about a factor of ten lower than the smallest experimental values for hydrocarbon diffusion in zeolites (*e.g.*, 50×10^{-23} m^2/s for *n*-hexane in 4A zeolite at 50°C, Table 12.2 in Ref. 33). Ordinary diffusion in microporous carbons, zeolites, and solids in general[33] should have a temperature dependence obeying the Eyring expression

$$D_S = D_S^0 \exp\left(-\frac{E_a}{RT}\right) \quad [26]$$

where E_a is the apparent activation energy for the diffusion process. The linearity of the corresponding Arrhenius plot (Fig. 4) for solvent diffusivities in MP cells is therefore consistent with solvent diffusion through a solid SEI. For the MP prototype cells, we find E_a = 9.5 kcal/mol, which compares well with values for interstitial diffusion in crystalline solids[30] as well as hydrocarbon diffusion in zeolites (*e.g.*, 8.5-9.5 kcal/mol for n-butane in 4A zeolite at 50°C, Table 12.2 in Ref. 19; 8-10 kcal/mol for aromatic hydrocarbons in silicalite, Fig. 14.16 in Ref. 33). The magnitudes of the diffusivity values, their conformance to the Eyring expression, and the activa-

Table III. Estimated values of D_s at various temperatures for HE and MP prototype cells, and corresponding infinite temperature diffusivities and activation energies from the Arrhenius plot in Fig. 4.

Cell prototype	Storage temp. (°C)	$D_s/10^{-23}$ (m^2/s)	D_S^0 (m^2/s)	E_a (kcal/mol)
HE	30	3.07		
	60	15.1		
			1.50×10^{-15}	10.7
MP	15	0.722		
	30	1.35		
	40	1.93		
	60	6.94		
			1.03×10^{-16}	9.50

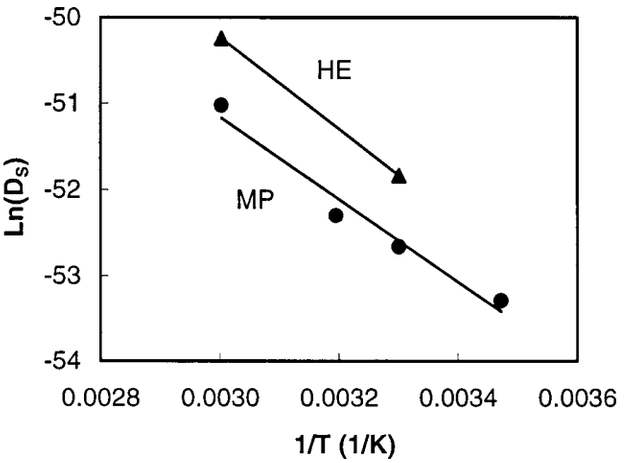

Figure 4. Arrhenius plot of solvent diffusivity *vs.* temperature for HE and MP prototype cells. Diffusivity values estimated from data in Fig. 2 and 3.

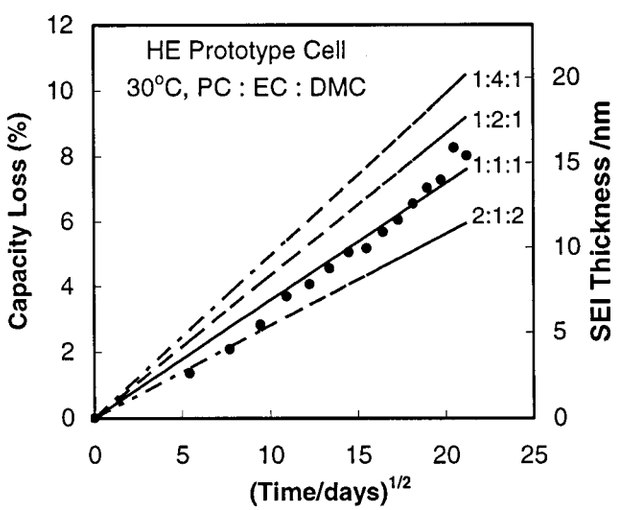

Figure 5. Predictions of capacity loss and SEI thickness as functions of time for different ratios of PC:EC:DMC in the electrolyte mixture for HE prototype cells. Symbols are measured capacity loss data[20] for an HE cell stored at 30°C with the SEI thickness estimate based on 1:1:1 PC:EC:DMC.

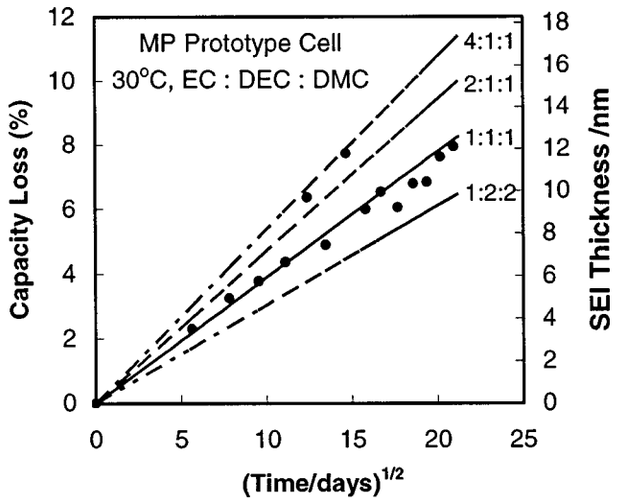

Figure 6. Predictions of capacity loss and SEI thickness as functions of time for different ratios of EC:DEC:DMC in the electrolyte mixture for MP prototype cells. Symbols are measured capacity loss data[20] for an MP cell stored at 30°C with the SEI thickness estimate based on 1:1:1 EC:DEC:DMC.

tion energy values are all reasonable and in accord with solvent diffusion through a crystalline, or perhaps microporous, SEI layer.

Broussely *et al.*[20] measured capacity losses for HE cells at only two temperatures, so we cannot prove Eyring behavior from the two HE data points in Fig. 4. Nonetheless, the slope of the line connecting these two points leads to $E_a = 10.7$ kcal/mol which agrees reasonably well with the value for the MP cells. At 30 and 60°C, the apparent solvent diffusivities in the HE cells are about 2.2 times greater than those in the MP cells. This offset could be explained by differing carbon surface areas in these cells, perhaps due to the difference in the methods used to prepare the composite anodes. In other words, if the accessible, electrochemically active carbon surface areas of the HE cells are actually 2.2 times larger than what we assumed (Table I), then the estimated solvent diffusivities would be identical for the HE and MP cells at the same temperature. The important point is that the solvent diffusivity values for two different Li-ion cell prototypes are in approximate agreement, lending further support to the solvent diffusion hypothesis.

Electrolyte composition.—It is well known in practice that the solvent composition in the electrolyte plays a critical role in controlling SEI formation, anode passivation, and long-term capacity fade. The solvent diffusion model provides a starting point for understanding and predicting the effect of solvent composition on SEI growth and capacity fade. For example, we may use the model to explore the effect of varying EC concentration on long-term capacity loss and SEI layer growth for cells under float potential conditions. Predictions for HE and MP prototype cells are given in Fig. 5 and 6. The symbols are the capacity loss data of Broussely *et al.*, with corresponding SEI thicknesses (solid lines) calculated under the assumption of 1:1:1 mixing (by volume) of the solvents used in the electrolytes. Capacity losses and SEI thicknesses for other solvent compositions are indicated by the dashed lines in each figure. As one might expect, the rates of capacity loss and SEI growth increase with the concentration of the reactive EC component in the electrolyte mixture.

Conclusions

We have presented a one-dimensional solvent diffusion model to explain the capacity loss of Li-ion cells during storage under float potentials at various temperatures. The primary result of the model is the prediction that capacity loss increases with the square root of time, in accord with experimental data.[20] Additional reasonable assumptions about the composition of the SEI lead to plausible estimates of SEI thickness, which also grows in proportion to the square root of time. The solvent diffusivity may be obtained from linear regression of capacity loss plotted *vs.* square root of time. An Arrhenius plot of diffusivities extracted from experimental data is linear, consistent with the behavior expected for temperature-dependent diffusivity of solvent through a solid, perhaps microporous SEI. The solvent diffusivities for two different cell prototypes differ by a constant factor that may be explained by uncertainties in details of cell design.

Although the model invokes many simplifying assumptions, it points toward the possibility of a new, realistic, tractable picture of the SEI on carbon anodes in Li-ion cells. The current ''working model'' is Peled's bilayer SEI,[7,8] consisting of an ultrathin, nonporous passivation barrier with non-negligible electronic conductivity, covered by a thick, macroporous, permeable layer with little relevance for passivation. Instead, we envision a single SEI layer with continuously varying properties including composition and porosity, much like the picture resulting from the simulations of Nainville *et al.*[34-37] A more sophisticated solvent diffusion model should be able to predict initial passivation characteristics as well as long-term capacity loss and SEI growth, all governed by the ability of reactive solvents to diffuse to within electron tunneling distance of the anode surface. One should be able to use this model to design ''good'' electrolytes by including reactive components that readily undergo reduction to form dense, low-porosity, insoluble products with low permeability to other electrolyte components.

Acknowledgments

The authors gratefully acknowledge financial support provided by the National Reconnaissance Office (NRO) under contract NRO-00-C-0134.

The University of South Carolina assisted in meeting the publication costs of this article.

List of Symbols

$A'A$,	empirical parameters in Eq. 1-4
A_{anode}	anode area, cm^2
$B'B$,	empirical parameters in Eq. 1-4
c	total molar concentration of the SEI phase, mol/cm^3
c_{eq}	equilibrium solvent molar concentration, mol/cm^3
c_P	product molar concentration in the SEI phase, mol/cm^3
c_S	solvent molar concentration, mol/cm^3
D_S^0	Arrhenius constant for diffusion, cm^2/s
D_S	solvent diffusivity in the SEI phase, cm^2/s
E_a	activation energy of the diffusion process, kcal/mol
k	proportionality constant in Eq. 1
L	SEI thickness, cm
L_0	initial SEI thickness, cm
M_i	molecular weight of component i, g/mol
$\mathcal{N}_L$	moles of lithium lost
$\mathcal{N}_0$	initial number of moles of lithium available for cycling
$N_{z,I}$	z component of molar flux of component I, mol/(s cm^2)
P	product formed as a result of solvent reduction reaction
r_I^σ	rate of production of component I by an interfacial reaction, g/s cm^3
R	gas constant, cal/mol K
S	solvent species
t	time, s
T	temperature, K
u	similarity transformation variable
x	fractional capacity loss
x_I	mole fraction of component I
X	SEI electronic conductance, mho
z	coordinate direction normal to the anode (cm)
Z_P	stoichiometric coefficient of Li in P

Greek

χ	SEI specific conductivity, S/cm^2
λ	a constant in the similarity solution

Subscripts

Li	lithium
S	solvent
P	solvent reduction product

References

1. P. Arora, R. E. White, and M. Doyle, *J. Electrochem. Soc.*, **145**, 3647 (1998).
2. R. J. Gummow, A. de Kock, and M. M. Thackeray, *Solid State Ionics*, **69**, 59 (1994).
3. J. M. Tarascon, W. R. McKinnon, F. Coowar, T. N. Bowmer, G. Amatucci, and D. Guyomard, *J. Electrochem. Soc.*, **141**, 1421 (1994).
4. D. Aurbach, M. D. Levi, K. Gamulski, B. Markovsky, G. Salitra, E. Levi, U. Heider, L. Heider, and R. Oesten, *J. Power Sources*, **81-82**, 472 (1999).
5. D. H. Jang, Y. J. Shin, and S. M. Oh, *J. Electrochem. Soc.*, **143**, 2204 (1996).
6. Y. Xia, Y. Zhou, and M. Yoshio, *J. Electrochem. Soc.*, **144**, 2593 (1997).
7. E. Peled, in *Lithium Batteries*, J. P. Gabano, Editor, Academic Press, New York (1983).
8. E. Peled, D. Golodnitsky, G. Ardel, C. Menachem, D. Bar Tow, and V. Eshkenazy, *Mater. Res. Soc. Symp. Proc.*, **393**, 209 (1995).
9. E. Peled, D. Golodnitsky, and G. Ardel, *J. Electrochem. Soc.*, **144**, L208 (1997).
10. Y. Ein-Eli, B. Markovsky, D. Aurbach, Y. Carmeli, H. Yamin, and S. Luski, *Electrochim. Acta*, **39**, 2559 (1994).
11. D. Aurbach, B. Markovsky, M. D. Levi, E. Levi, A. Schechter, M. Moshkovich, and Y. Cohen, *J. Power Sources*, **81-82**, 95 (1999).
12. D. Aurbach, B. Markovsky, I. Weissman, E. Levi, and Y. Ein-Eli, *Electrochim. Acta*, **45**, 67 (1999).
13. D. Aurbach, *J. Power Sources*, **89**, 206 (2000).
14. D. Aurbach, in *Advances in Lithium-Ion Batteries*, W. A. van Schalkwijk and B. Scrosati, Editors, pp. 7-77, Academic Press, New York (2002).
15. D. Zane, A. Antonini, and M. Pasquali, *J. Power Sources*, **97-98**, 146 (2001).
16. M. Dollé, S. Grugeon, B. Beaudoin, L. Dupont, and J.-M. Tarascon, *J. Power Sources*, **97-98**, 104 (2001).
17. M. Inaba, Z. Siroma, A. Funabiki, and Z. Ogumi, *Langmuir*, **12**, 1535 (1996).
18. Z. Ogumi, K.-K. Jeong, M. Inaba, and T. Abe, *Macromol. Symp.*, **156**, 195 (2000).
19. D. Alliata, R. Kotz, P. Novak, and K. Sieganthaler, *Electrochem. Commun.*, **2**, 436 (2000).
20. M. Broussely, S. Herreyre, P. Biensan, P. Kasztejna, K. Nechev, and R. J. Staniewicz, *J. Power Sources*, **97-98**, 13 (2001).
21. M. Broussely, in *Advances in Lithium-Ion Batteries*, W. A. van Schalkwijk and B. Scrosati, Editors, pp. 393-432, Academic Press, New York (2002).
22. J. C. Slattery, *Advanced Transport Phenomena*, Cambridge University Press, Cambridge, MA (1999).
23. C. R. Yang, Y. Y. Wang, and C. C. Wan, *J. Power Sources*, **72**, 66 (1998).
24. D. Aurbach, Y. Gofer, M. Ben-Zion, and P. Aped, *J. Electroanal. Chem. Interfacial Electrochem.*, **339**, 451 (1992).
25. T. Li and P. B. Balbuena, *Chem. Phys. Lett.*, **317**, 421 (2000).
26. K. Peng, L. Wang, and J. Slattery, *J. Vac. Sci. Technol. B*, **14**, 3317 (1996).
27. J. P. Olivier and M. Winter, *J. Power Sources*, **97-98**, 151 (2001).
28. B. A. Johnson and R. E. White, *J. Power Sources*, **70**, 48 (1998).
29. P. Ramadass, A. Durairajan, B. Haran, R. E. White, and B. N. Popov, *J. Electrochem. Soc.*, **149**, A54 (2001).
30. C. R. Barrett, W. D. Nix, and A. S. Tetelman, *The Principles of Engineering Materials*, pp. 150-155, Prentice-Hall, Englewood Cliffs, NJ (1973).
31. K. A. Hirasawa, T. Sato, H. Asahina, S. Yamaguchi, and S. Mori, *J. Electrochem. Soc.*, **144**, L81 (1997).
32. A. C. Chu, J. Y. Josefowicz, and G. C. Farrington, *J. Electrochem. Soc.*, **144**, 4161 (1997).
33. J. Kärger and D. M. Ruthven, *Diffusion in Zeolites*, Wiley, New York (1992).
34. I. Nainville, A. Lemarchand, and J.-P. Badiali, *Phys. Rev. E*, **53**, 2537 (1996).
35. I. Nainville, A. Lemarchand, and J.-P. Badiali, *Electrochim. Acta*, **41**, 1855 (1996).
36. I. Nainville, A. Lemarchand, and J.-P. Badiali, *Electrochim. Acta*, **41**, 2855 (1996).
37. M. Lafage, D. Windel, V. Russier, and J.-P. Badiali, *Electrochim. Acta*, **42**, 2841 (1997).